SPECIAL TOPIC — Acoustics

Controls of pass-bands in asymmetric acoustic transmission*

Hong-Xiang Sun(孙宏祥)[1,2,3,†], Shu-Yi Zhang(张淑仪)[1,‡], and Shou-Qi Yuan(袁寿其)[2]

[1] *Laboratory of Modern Acoustics, Institute of Acoustics, Collaborative Innovation Center of Advanced Microstructures, Nanjing University, Nanjing* 210093, *China*

[2] *Research Center of Fluid Machinery Engineering and Technology, Jiangsu University, Zhenjiang* 212013, *China*

[3] *State Key Laboratory of Acoustics, Institute of Acoustics, Chinese Academy of Sciences, Beijing* 100190, *China*

(Received 13 November 2015; revised manuscript received 20 March 2016; published online 25 October 2016)

The controls of the pass-bands in an asymmetric acoustic transmission system are investigated numerically and experimentally, and the system consists of a periodical rectangular grating and two uniform brass plates in water. We reveal that the pass-band of the asymmetric acoustic transmission is closely related to the grating period, but is affected slightly by the brass plate thickness. Moreover, the transmittance can be improved by adjusting the grating period and other structural parameters simultaneously. The control method of the system has the advantages of wider frequency range and simple operation, which has great potential applications in ultrasonic devices.

Keywords: asymmetric acoustic transmission, pass-band control, grating diffraction, Lamb mode

PACS: 43.35.+d, 43.20.+g **DOI:** 10.1088/1674-1056/25/12/124313

1. Introduction

In natural materials, energy fluxes generally propagate reciprocally. In the past decade, considerable efforts have been devoted to the investigations on the rectifications of different energy fluxes by using specially designed artificial structures, such as thermal flux,[1,2] electromagnetic waves,[3–6] and solitary waves.[7] Inspired by the great applications of these systems, the realization of the asymmetric acoustic transmission (AAT)[8] has become a hot topic due to its potential applications in a variety of important fields, such as acoustic rectifier, acoustic diode, and medical ultrasound diagnosis and therapy.

The first AAT model is composed of a nonlinear medium and a band gap phononic crystal,[9] and instead it may be comprised of other nonlinear medium, such as a granular crystal[10] and an active acoustic metamaterial.[11] Because of the intrinsic limitations of nonlinear effects, including the narrow pass-band and low transmission efficiency, etc., more attention has been paid to the investigations on the AAT by using linear acoustic structures, such as a resonant ring cavity structure,[12] grating structures,[13–19] phononic crystals,[20–23] and other types of structures.[24–28] The above linear acoustic structures have remarkably enhanced the transmission efficiencies and improved performances of the AATs.

Practically, the controllable performances of the AAT could open great possibilities for engineering applications. Thus, the relationships between the structural parameters and the properties of the AAT have been simulated numerically by the finite element method, such as the propagation direction of the transmitted beam[17,19] and switch.[20,24] Moreover, the influence of the overall size of structure on the frequency band has also been preliminarily discussed,[15] but the quantitative relationship between the frequency band and specific parameters has not been studied, and little experimental work has been published so far in this field. These problems restrict the application range and the development of tunable AAT devices.

In this article, we investigate the control mechanism of the pass-band of the AAT in an acoustic system which consists of a periodic grating and two uniform plates in water. We realize the quantitative control of the pass-band by the grating period, and improve the transmittance by adjusting the grating period and other structural parameters simultaneously. The experimental results agree well with the numerical simulations.

2. Experimental and numerical models

2.1. Experimental sample and set-up

As shown schematically in Fig. 1(a), the sample consists of a periodic rectangular brass grating and two uniform brass plates with the same sizes in water, and the two uniform brass plates are adopted to optimize the rectifying ratio of the AAT.[16] The width (w) and length (l) of the grating are 72 mm and 120 mm, and for both brass plates, the width (w_1) and length (l_1) are 200 mm and 120 mm respectively. Moreover, the grating period (a), the width (s), the thickness (d) of each stripe of the grating, the thickness of the plate (h), the

*Project supported by the National Basic Research Program of China (Grant No. 2012CB921504), the Major Program of the National Natural Science Foundation of China (Grant No. 51239005), the National Natural Science Foundation of China (Grant Nos. 11174142 and 11404147), the Natural Science Foundation of Jiangsu Province, China (Grant No. BK20140519), the China Postdoctoral Science Foundation (Grant No. 2015M571672), the Training Project of Young Backbone Teachers of Jiangsu University, China, and the Research Fund for Advanced Talents of Jiangsu University, China (Grant No. 13JDG106).

†Corresponding author. E-mail: jsdxshx@ujs.edu.cn

‡Corresponding author. E-mail: zhangsy@nju.edu.cn

© 2016 Chinese Physical Society and IOP Publishing Ltd

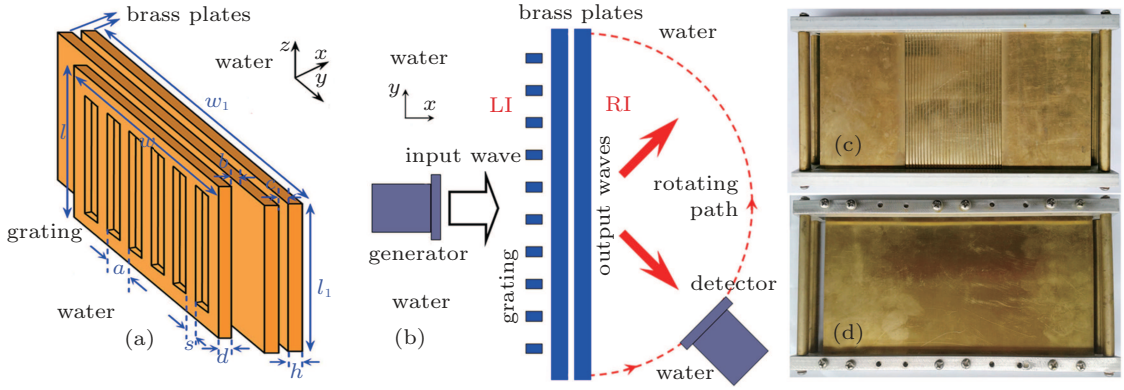


Fig. 1. (color online) Schematic diagrams of (a) sample and (b) experimental set-up, and photographs of (c) left and (d) right sides of sample.

distance between the grating and plate (b), and that between the plates (c) are 2.4 mm, 0.6 mm, 1.0 mm, 1.0 mm, 0.5 mm, and 0.5 mm, respectively.

Figure 1(b) shows the diagram of the experimental set-up. The sample is placed between a pair of ultrasonic generation and detection transducers each with a central frequency of 500 kHz, bandwidth of 250 kHz–1100 kHz, and diameter of 20 mm. The generation transducer is aligned normally towards the sample with a distance of 12 cm. On the other side, the detection transducer scans around the sample in a semicircle. The abbreviations LI and RI refer to the incident acoustic waves emanated from the grating and plates sides of the sample respectively. In the experiment, we measure the transmittance spectra by integrating the total energy flux of the transmitted acoustic beams, and the photographs for both sides of the experimental sample are shown in Figs. 1(c) and 1(d), respectively.

2.2. Numerical model

Moreover, the numerical simulations are carried out by the finite element method based on COMSOL Multiphysics software. The material parameters in the present simulations are adopted as follows: the density $\rho_{\rm b} = 8400$ kg/m^3, the longitudinal wave velocity $c_{\rm lb} = 4400$ m/s and the transversal wave velocity $c_{\rm tb} = 2200$ m/s for brass; and the density $\rho_{\rm w} = 998$ kg/m^3 and the longitudinal wave velocity $c_{\rm lw} = 1483$ m/s for water. The width of the incident acoustic plane wave is assumed to be 20 mm, which is the same as the diameter of the generation transducer.

3. Properties of AAT

3.1. Transmission spectra

Figure 2(a) shows the numerical (NU) and experimental (EX) results of the transmittance spectra. In the numerical results, the pass-band of LI is 612 kHz–763 kHz, which is shown in a shaded region, and the maximum of the transmittance reaches 0.80 at 660 kHz. However, the transmittance of RI is almost zero, and therefore the transmittance spectra exhibit remarkable AAT behavior. Similarly, the experimental transmittance spectra also demonstrate the strong asymmetric behavior, but the width of the pass-band of LI is narrower than the numerical result, and the measured amplitudes are much smaller in the frequency region of 673 kHz–763 kHz. The main reason responsible for the discrepancies between the numerical and experimental results may be that the geometrical and material parameters used in both cases are different due to the fact that the parameters in the experiments are not accurately determined.

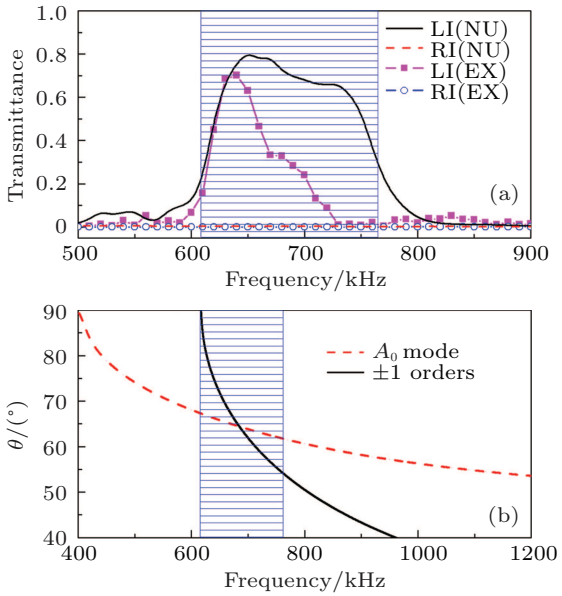


Fig. 2. (color online) (a) Numerical (NU) and experimental (EX) transmittance spectra through the sample, and (b) distributions for leaky angles of A_0 mode and diffracted angles of ± 1 orders.

3.2. Physical mechanism of AAT

In order to investigate the AAT mechanism, we theoretically calculate the leaky angle of the Lamb wave in a brass plate immersed in water based on Snell's law $\theta = \arcsin(c_{\rm lw}/c_{\rm p})$, where θ is the angle between the leaky direction of the Lamb wave and the normal direction of the brass plate, and $c_{\rm p}$ is the phase velocity of the Lamb wave in the brass plate immersed in water. It is noted whether the energy of the Lamb wave could leak into water in the form of the bulk wave, which is most likely to be dependent on its phase

velocity (in contrast to the sound velocity of water).

Figure 2(b) shows the distributions of the diffracted angle of the ±1-orders from the grating[29] with the period 2.4 mm and the leaky angle of asymmetric zero-order Lamb mode (A_0) in a brass plate with the thickness 1.0 mm in water. We find that the energy of the A_0 mode leaks into the water with the incident frequencies exceeding 400 kHz and different propagation angles. Therefore, it is necessary to point out that the A_0 mode in the brass plate could be excited by the external bulk wave with the critical frequency and certain critical angle.[30]

As shown in Fig. 2(b), the angle curve of the A_0 mode intersects that of the ±1-orders at 660 kHz, and that the pass-band of the AAT appears around the intersection point. It indicates that as the diffracted angle of the ±1-orders is the same as or close to the leaky angle of the A_0 mode, the ±1-orders can transmit through the brass plates. It is therefore obtained that the pass-band of the AAT is mainly determined by the diffracted angle of the ±1-orders and the leaky angle of the A_0 mode, of which the two are related to the parameters a and h, respectively.

4. Controls of pass-bands of AAT

4.1. Grating period

Next, we simulate the transmittance spectra by magnifying each grating period (a) and thickness of the plate (h) n times, in which n ranges from 0.5 to 2, and the other parameters remain constant.

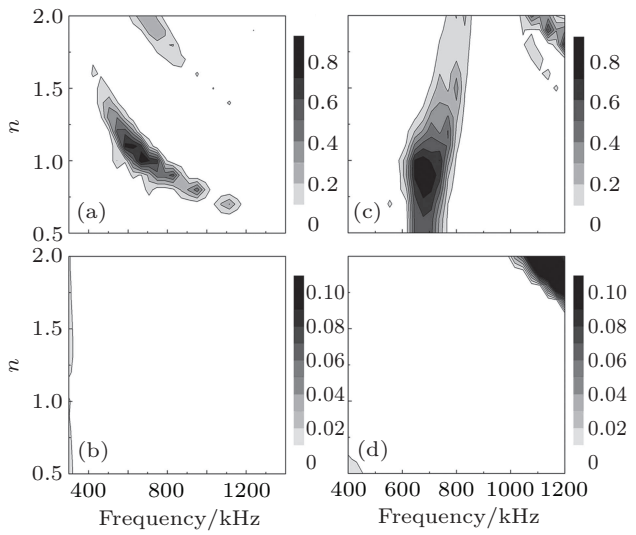


Fig. 3. Numerical transmittance spectra by magnifying a value n times for (a) LI and (b) RI, and h value n times for (c) LI and (d) RI.

Figure 3(a) shows the transmittance spectra of LI by magnifying the a value n times, in which the transmittance is plotted by the gray scale. When n ranges from 0.7 to 1.6, the pass-band of the AAT greatly moves to the low frequency region with the increase of n, and the bandwidth almost remains unchanged with n ranging from 0.9 to 1.3. However, when n is larger than 1.3, the bandwidth gradually narrows, and when n increases to 1.6, the low cut-off frequency of the pass-band is about 400 kHz, which is the same as that of the A_0 mode in the brass plate [Fig. 2(b)]. In addition, the second pass-band appears in the high frequency region with$n$ larger than 1.6, and when n reaches 1.65, the first pass-band disappears, and the second pass-band becomes wider. Moreover, when n reduces to 0.7, the pass-band of the AAT disappears. On the other hand, for RI, there is no transmittance in the frequency range of the AAT as shown in Fig. 3(b). Therefore, we deduce that the pass-band of the AAT is closely related to the grating period.

4.2. Plate thickness

Figure 3(c) shows the transmittance spectra of LI by magnifying the h value n times. It is found that the pass-band of the AAT shifts slightly to the high frequency region with the increase of n, indicating that the pass-band of the AAT is slightly affected by h. Similarly, the transmittance in the frequency range of the AAT is also very weak for RI, as shown in Fig. 3(d).

4.3. Control mechanism of pass-bands of AAT

To investigate the mechanism of the variation of the pass-band of the AAT, we further calculate the distributions of the leaky angle of the A_0 mode in the brass plate and the diffracted angle of different orders from the grating by separately magnifying each of a [$n(a)$] and h [$n(h)$] values n times, which are shown in Figs. 4(a) and 4(b), respectively, in which the shaded regions represent the pass-bands of the AAT.

It is found from Fig. 4(a) that with the increase of $n(a)$, the angle curve of the A_0 mode remains unchanged, but the angle curves of the ±1-orders move to the low frequency region, and so do the intersection points of the ±1-orders and the A_0 mode. Therefore, the pass-bands of the AAT shift to the low frequency region with the increase of $n(a)$, and the pass-bands of the AAT can be controlled by the grating period.

Moreover, when $n = 1.8$ or more, there is no intersection point between the curves of the ±1-orders and the A_0 mode, so the pass-band of the AAT disappears in the low frequency range. However, there is an intersection point of the ±2-order diffractions and the A_0 mode located at about 800 kHz, and the second pass-band of the AAT appears in the region around this frequency. These phenomena agree well with the results in Fig. 3(a).

As shown in Fig. 4(b), with the increase of $n(h)$, the angle curve of the ±1-orders remains constant, but the angle curves of the A_0 mode shift to the low frequency region, and the intersection points of the ±1-orders and the A_0 mode move slightly to the high frequency region, which induces the pass-bands of the AAT to shift slightly. The results agree well with those

in Fig. 3(c). Thus, the pass-band of the AAT is slightly influenced by the plate thickness.

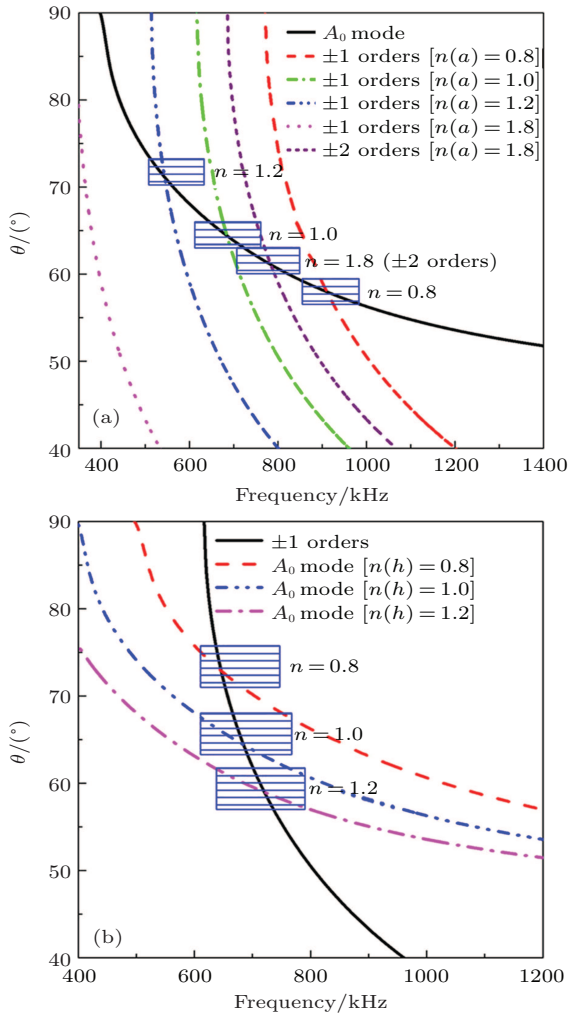


Fig. 4. (color online) Distributions for leaky angles of A_0 mode and diffracted angles of different orders by magnifying (a) a and (b) h values n times.

Based on the aforementioned discussion, we can conclude that the pass-band of the AAT is mainly determined by the grating period, and is slightly affected by the plate thickness, which is in agreement with the numerical transmittance spectra [Figs. 3(a) and 3(c)].

4.4. Grating period and other parameters

In order to improve the transmittance of the AAT, we investigate the AAT characteristics by magnifying each of the values of a and four other kinds of parameters (h; s and d; b and c; and h, s, d, b, and c) n times simultaneously, and the corresponding transmittance spectra for LI are shown Figs. 5(a)–5(d), respectively. It is shown from Figs. 5(a) and 5(d) that the bandwidth of the AAT almost remains unchanged by changing both parameters a and h. Moreover, the transmittances [Figs. 5(a)–5(d)] in the low and/or high frequency regions are stronger than those with magnifying only a [Fig. 3(a)]. In particular, as shown in Fig. 5(d), the pass-band of the AAT moves to the low frequency region gradually with the increase of the overall size of the system, while the bandwidth and transmittance remain constant. Therefore, we obtain that the transmittance of the AAT can be improved by adjusting the grating period and other structural parameters simultaneously.

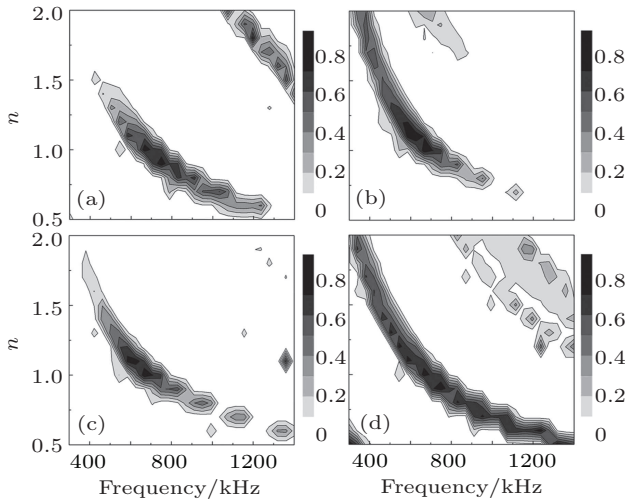


Fig. 5. Numerical transmittance spectra for LI by magnifying n times each of the values of a and other parameters (a) h, (b) s and d, (c) b and c, and (d) h, s, d, b, and c.

Figure 6 shows the distributions of the leaky angles of the A_0 mode and the diffracted angles of the ±1-orders by separately magnifying both parameters a and h values 0.8, 1.0, and 1.2 times separately. It is seen from Fig. 6 that with the increases of a and h, the curves of the ±1-orders and A_0 mode move to the lower frequency region simultaneously and with almost the same scale. Therefore, the pass-bands of the AAT shift to the lower frequency region at the same time, and the bandwidths of the AAT with different magnifications are almost the same, which agrees well with the results in Figs. 5(a) and 5(d).

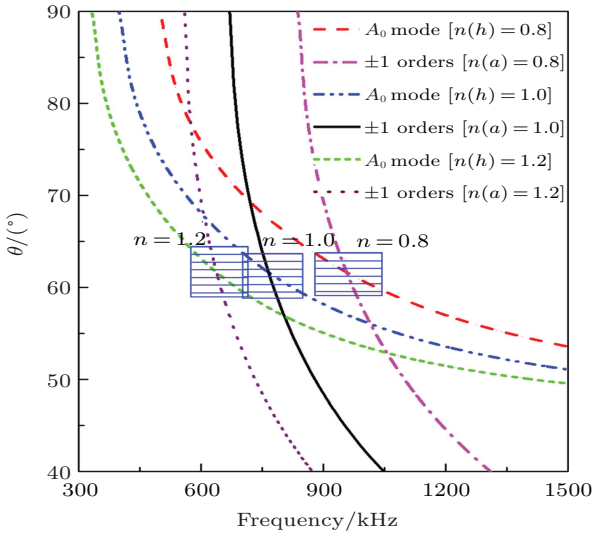


Fig. 6. (color online) Distributions for leaky angles of A_0 mode and diffracted angles of ±1-orders by magnifying both a and h values n times.

5. Experimental verifications

Furthermore, we experimentally measure the transmittance spectra for LI and RI with 0.8 and 1.2 times the parameters a and h, respectively, and the parameters a and h separately, as shown in Figs. 7(a), 7(c), and 7(e). The corresponding numerical results are also displayed in Figs. 7(b), 7(d), and 7(f) for comparison. It is shown that the variations of the pass-bands of the AAT in the experiment are well consistent with the numerical results. In addition, comparing Figs. 7(a) with 7(e), we find that the measured transmittance of the pass-band of LI by 0.8 times both a and h are larger than that of a, which agrees well with the results in Figs. 3(a) and 5(a).

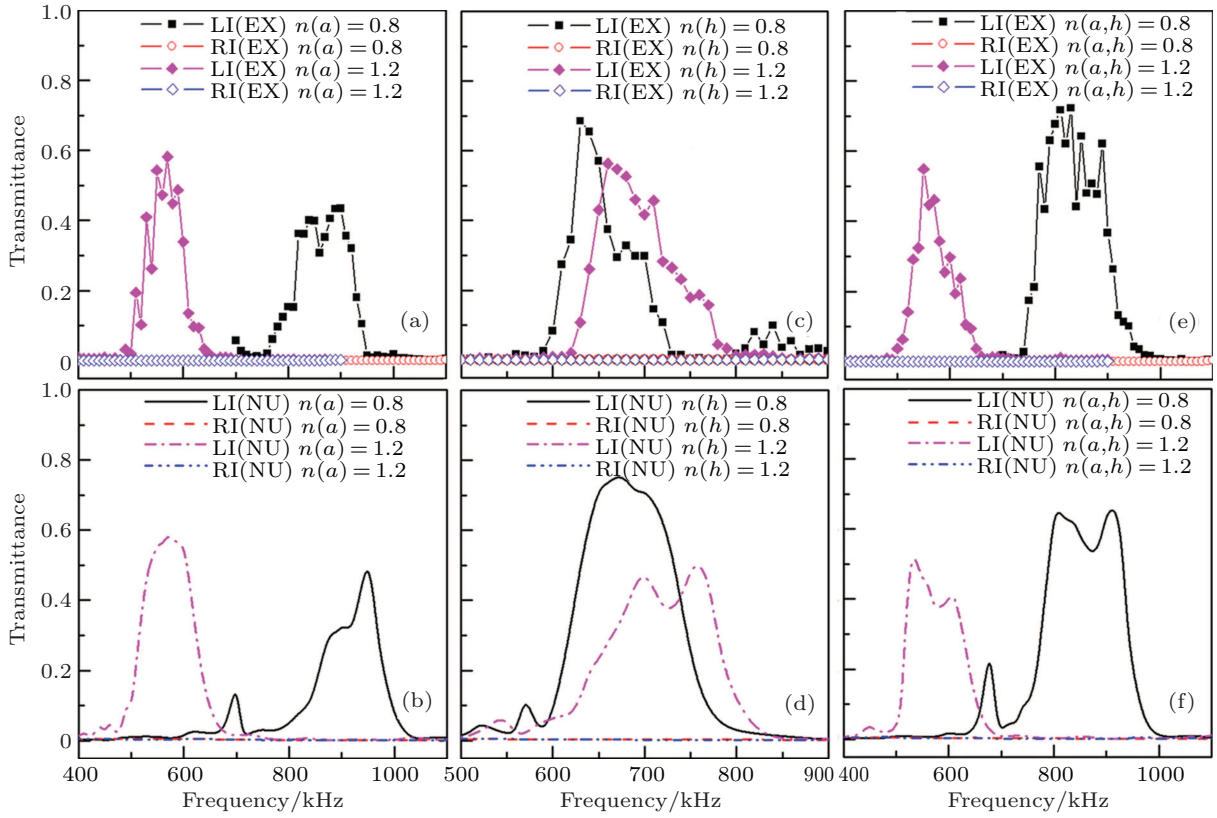


Fig. 7. (color online) Experimental and numerical transmittance spectra by using 0.8 and 1.2 times values of ((a) and (b)) a, ((c) and (d)) h, and ((e) and (f)) both a and h.

6. Conclusions

We investigate the control mechanism of the pass-band of the AAT in an acoustic system numerically and experimentally. The results show that the pass-band of the AAT is closely related to the grating period which determines the diffracted angle of the ± 1-orders to match the leaky angle of the A_0 mode in the plates. Moreover, the transmittance of the AAT can be improved by adjusting the grating period and other structural parameters simultaneously. The numerical results are verified by the experimental measurements, and agree well with each other. The control mechanism has the advantages of wider frequency range and simple operation, which has important scientific significances and potential applications in the tunable unidirectional acoustic devices.

References

[1] Li B, Wang L and Casati G 2004 *Phys. Rev. Lett.* **93** 184301
[2] Chang C W, Okawa D, Majumdar A and Zettl A 2006 *Science* **314** 1121
[3] Haldane F D M and Raghu S 2008 *Phys. Rev. Lett.* **100** 013904
[4] Yu Z and Fan S 2009 *Nat. Photon.* **3** 91
[5] Feng L, Ayache M, Huang J, Xu Y L, Lu M H, Chen Y F, Fainman Y and Scherer A 2011 *Science* **333** 729
[6] Fan L, Wang J, Varghese L T, Shen H, Niu B, Xuan Y, Weiner A M and Qi M 2012 *Science* **335** 447
[7] Nesterenko V F, Daraio Herbold C E B and Jin S 2005 *Phys. Rev. Lett.* **95** 158702
[8] Liang B, Yuan Y and Cheng J C 2015 *Acta Phys. Sin.* **64** 094305 (in Chinese)
[9] Liang B, Yuan B and Cheng J C 2009 *Phys. Rev. Lett.* **103** 104301
[10] Boechler N, Theochari G and Daraio C 2011 *Nat. Mater.* **10** 665
[11] Popa B I and Cummer S A 2014 *Nat. Commun.* **5** 3398
[12] Fleury R, Sounas D L, Sieck C F, Haberman M R and Alù A 2014 *Science* **343** 516
[13] He Z J, Peng S S, Ye Y T, Dai Z W, Qiu C Y, Ke M Z and Liu Z Y 2011 *Appl. Phys. Lett.* **98** 083505
[14] Tanaka Y, Murai T and Nishiguchi N 2012 *J. Appl. Phys.* **111** 024507
[15] Sun H X, Zhang S Y and Shui X J 2012 *Appl. Phys. Lett.* **100** 103507
[16] Sun H X and Zhang S Y 2013 *Appl. Phys. Lett.* **102** 113511
[17] Jia H, Ke M Z, Li C H, Qiu C Y and Liu Z Y 2013 *Appl. Phys. Lett.* **102** 153508
[18] Sun H X, Yuan S Q and Zhang S Y 2015 *Appl. Phys. Lett.* **107** 213505
[19] Sun H X, Zhang S Y, Yuan S Q and Xia J P 2016 *Appl. Phys. A* **122** 328
[20] Li X F, Ni X, Feng L, Lu M H, He C and Chen Y F 2011 *Phys. Rev. Lett.* **106** 084301

[21] Cicek A, Kaya O A and Ulug B 2012 *Appl. Phys. Lett.* **100** 111905
[22] Oh J H, Kim H W, Ma P S, Seung H M and Kim Y Y 2012 *Appl. Phys. Lett.* **100** 213503
[23] Huang Y L, Sun H X, Xia J P, Yuan S Q and Ding X L 2016 *Appl. Phys. Lett.* **109** 013501
[24] Li Y, Liang B, Gu Z M, Zou X Y and Cheng J C 2013 *Appl. Phys. Lett.* **103** 053505
[25] Zhu Y F, Zou X Y, Liang B and Cheng J C 2015 *Appl. Phys. Lett.* **106** 173508
[26] Danworaphong S, Kelf T A, Matsuda O, Tomoda M, Tanaka Y, Nishiguchi N, Wright O B, Nishijima Y, Ueno K, Uodkazis S and Misawa H 2011 *Appl. Phys. Lett.* **99** 201910
[27] Zanjani M B, Davoyan A R, Mahmoud A M, Engheta N and Lukes J R 2014 *Appl. Phys. Lett.* **104** 081905
[28] Gu Z M, Liang B, Zou X Y, Yang J, Li Y, Yang J and Cheng J C 2015 *Appl. Phys. Lett.* **107** 213503
[29] Twersky V 1962 *IEEE Trans. Anten. Propag.* **10** 737
[30] Bhattacharya M C, Guy R W and Crocker M J 1971 *J. Sound Vib.* **18** 157